THE UNIVERSITY OF

WARWICK

warwickpublicationswrap

highlight your research

http://go.warwick.ac.uk/lib-publications

Ion beam sputtered surface dynamics investigated with two-time correlation functions: a model study

Oier Bikondoa[1,2], Dina Carbone[3], Virginie Chamard[4] & Till Hartmut Metzger[5]

[1]XMaS UK-CRG Beamline at the ESRF. B. P. 220. F-38043 Grenoble cedex 09 (France)

[2]Department of Physics, University of Warwick, Gibbet Hill Road, Coventry, CV4 7AL, UK

[3]European Synchrotron Radiation Facility, 6 rue Jules Horowitz, B. P. 220, F-38043 Grenoble cedex 09 (France)

[4]Institut Fresnel, CNRS, Aix-Marseille Université, Ecole Centrale Marseille, Campus de Saint-Jérome, 13013 Marseille cedex 20, France

[5]Max Planck Institute of Colloids and Interfaces, D-14424 Potsdam, Germany

E-mail: `oier.bikondoa@esrf.fr`

Abstract.

Ion beam sputtering is a widely used technique to obtain patterned surfaces. Despite the large use of this approach on different materials to create surface nanostructures, the theoretical model to explain the time evolution of the erosion process is still debated. We show with the help of simulations, that two-time correlation functions can serve to assess the validity of different models. These functions can be measured experimentally with the X-ray photon correlation spectroscopy technique.

PACS numbers: 81.16.Rf,62.23.St,05.65.+b

Erosion of surfaces by ion beams can induce self-organisation processes leading to the formation of arrays of nanostructures [1]. Since the observation of periodic ripples on sputtered surfaces, back in the sixties, ion beam sputtered surfaces have been extensively studied, especially after Facsko *et al.* [2] demonstrated the capabilities of the technique to create ordered nanodot patterns on a semiconductor (GaSb) surface. A special issue of *J. Phys: Cond. Matt.* has been dedicated to the subject [3] and there are several comprehensive reviews in the literature [4, 5, 6, 7].

The temporal evolution of the surface morphology during ion beam sputtering (IBS) is determined by a complex interplay between different physical mechanisms that tend to roughen or smooth the surface. This evolution depends profoundly on parameters such as the beam energy, angle of incidence of the ion beam on the surface, substrate temperature, etc. There is both a fundamental and a technological interest in understanding how these parameters influence the surface morphology. X-ray methods have been proven particularly convenient for the experimental study of nanopatterned surfaces [8, 9]. They allow to characterise the surface morphology during erosion, *in situ* and in real time. They have the advantage with respect to direct imaging techniques (i.e. atomic force, scanning tunnelling, scanning or transmission electron microscopies) in that no special sample preparation is required and that the information obtained is not restricted to the surface. Sensitivity to the surface and subsurface regions is achieved by using grazing incidence techniques such as grazing incidence small angle X-ray scattering (GISAXS) or diffraction (GID).

In general, typical structures generated by IBS include dots and ripples [3]. For both types of nanostructures, coarsening can occur during the erosion process, i. e. the mean distance between the nanostructures (pattern wavelength) increases with time. Under normal incidence sputtering, saturation of the dot pattern wavelength has been observed for different surfaces such as Si(001), Si(111), Ge(001) and GaSb(001) [9]. Diverse studies indicate that on monoelemental surfaces the redistribution of sputtered material is a fundamental process controlling pattern formation [10, 11, 12, 13, 14, 15]. A physical model in which mass redistribution is included in a systematic and consistent way has been put forward very recently [16, 17]. The case of bielemental surfaces or monoelemental surfaces with impurities is more complex because the evolution of the height and composition modulations are coupled [18, 19, 20]. Certainly, if IBS is to be used as a nanopatterning method, it is essential to know when coarsening occurs, if the pattern wavelength saturates and if the pattern ordering may be enhanced by further sputtering. Coarsening and wavelength saturation are also important issues for the theoretical understanding of IBS, as they are not predicted by all the models [7].

When the pattern wavelength saturation has been reached, the surface morphology is in dynamical equilibrium: the statistical ensemble average characteristics, such as the roughness or pattern wavelength, may remain unchanged but the surface is still evolving due to erosion. Obtaining experimental information about the surface evolution in the saturation regime is a challenging task. Conventional GID or GISAXS measurements provide information about the ensemble average properties of the surface at a given

time and are insensitive to local variations of the surface morphology [9]. If the ensemble averaged characteristics do not change in time, the results of GID or GISAXS measurements will not change. This problem can be bypassed by using the XPCS technique, which exploits the characteristics of GISAXS or GID patterns obtained with a coherent X-ray beam [21]. Under coherent illumination, the diffracted intensity shows a graininess called speckle. The speckle pattern depends on the **exact** (i.e. non-ensemble averaged) spatial surface morphology at a given time [22]. If the surface morphology varies with time, even if the statistical properties are identical, the corresponding speckle pattern will change. Information about the dynamics of the system can be extracted from the speckle intensity fluctuations. This is the basis of the X-ray photon correlation spectroscopy technique (XPCS) [23, 24, 25, 26]. XPCS is the equivalent of the dynamic light scattering technique [27] using X-rays and is generally used to study the dynamical properties of soft and hard condensed matter systems: glasses, colloidal suspensions, liquid surfaces, phase transitions, etc. [25].

In the kinematical approximation of scattering, i.e., neglecting multiple scattering events, the scattered intensity from a nanostructured surface, at a momentum transfer $\boldsymbol{q}$ at time t, is proportional to an interference function:

$$I\left(\boldsymbol{q}, t\right) \propto \sum_{m,n} \mathrm{e}^{i\boldsymbol{q}\cdot(\boldsymbol{R_m} - \boldsymbol{R_n})} \tag{1}$$

where $\boldsymbol{R_m}$ denotes the position of a nanostructure and the sum is done for all the nanostructures. The interference function in reciprocal space is the Fourier transform of the electron density autocorrelation function in real space [9, 28]:

$$I\left(\boldsymbol{q}, t\right) \propto \int C\left(\boldsymbol{r}, t\right) \mathrm{e}^{i\boldsymbol{q}\cdot\boldsymbol{r}} dV \tag{2}$$

where

$$C\left(\boldsymbol{r}, t\right) = \int \rho\left(\boldsymbol{r}', t\right) \rho\left(\boldsymbol{r} + \boldsymbol{r}', t\right) dV' \tag{3}$$

is the spatial autocorrelation function of the electron density ρ ‡. In the case of a surface, ρ can be expressed in terms of the height at a point (x, y) and time t by:

$$\rho\left(\boldsymbol{r}, t\right) = \rho_0 \mathrm{H}\left[h\left(x, y, t\right) - z\right] \tag{4}$$

$\mathrm{H}\left(\alpha\right)$ is Heaviside's unit step function ($\mathrm{H}\left(\alpha \leq 0\right) = 0$ and $\mathrm{H}\left(\alpha > 0\right) = 1$). ρ_0 is the mean electron density of the material. We have explicitly included the dependence on the time t of the scattered intensity $I\left(\boldsymbol{q}, t\right)$ and the height-height correlation function $C\left(\boldsymbol{r}, t\right)$ because the contour of the surface is continuously changing during IBS. Equation (1) is correct for a sample illuminated with a perfectly coherent beam. When using partially coherent illumination [21], as in conventional GISAXS and GID experiments, the intensity of different coherence volumes must be summed incoherently and the interference function of Eq. (1) has to be statistically averaged over all possible spatial

‡ Eq. (2) is mathematically equivalent to the power spectrum density that is often used to analyse scanning probe microscopy images. See Ref. [9] for some technical remarks.

configurations. In this case, the diffraction pattern contains information on the average correlations only [28]. In the saturation regime, where the average correlations do not change, the scattered intensity from a IBS sample illuminated incoherently and measured at two different times will be equal. When coherent illumination is used, the intensity fluctuates about the average intensity and the envelope of the speckle distribution coincides with the GISAXS or GID patterns obtained with a partially coherent beam. The intensity fluctuations of the speckles depend on the exact spatial arrangement of the nanostructures. Thus, the intensity fluctuations measured in an XPCS experiment are related to the temporal evolution of the exact spatial height-height correlations and to the dynamic structure factor. This information can be used to determine how the surface morphology evolves (i.e. if the pattern saturates into an steady state or not, if the pattern evolution is chaotic, etc.) and to compare with the predictions of theoretical models.

One theoretical approach used to describe surfaces during IBS, and which can predict coarsening and saturation, is the continuum theory [7]. In this approach, the surface evolution is described in terms of differential equations of the height. These equations are generally not linear and do not have analytical solutions, requiring the use of either analytical approximations or numerical methods for their study. Numerically, those models allow to access large spatial (i.e. micrometer range) and temporal (thousands of seconds) scales and are not very computationally demanding.

Hereafter we analyse two equations that have been put forward to describe the formation of nanodots during normal incidence IBS on monoelemental materials. Facsko and co-workers [29] showed that the evolution of the surface morphology during IBS is qualitatively reproduced by the damped Kuramoto-Sivashinsky (DKS) equation [30]. The proposed DKS equation is:

$$\frac{\partial h}{\partial t} = -v_0 - \alpha h + \nu \nabla^2 h - D_{eff} \nabla^4 h + \frac{\lambda}{2} \left(\nabla h \right)^2 + \eta \tag{5}$$

where v_0 is the constant erosion velocity, α the damping constant, ν the surface tension, D_{eff} the effective diffusion coefficient accounting for thermal and erosion induced diffusion, $\lambda/2$ is related to the tilt dependent sputtering yield and η is a noise term. v_0 can be eliminated from the equation by a suitable redefinition of the surface height (see Ref. [29] for details). It has been suggested that the damping term αh arises from the redeposition of sputtered material [29]. However, the physical plausibility of such term and the validity of Eq. (5) for IBS is still debated [7, 31].

Another model, proposed by Castro *et al.* [32], considers two fields, the surface height and the concentration of mobile atoms on the surface, whose temporal evolution is described by a set of two coupled nonlinear differential equations. From this two-field continuum model, a single effective equation for the height is derived:

$$\frac{\partial h}{\partial t} = -\nu \nabla^2 h - \mathcal{K} \nabla^4 h + \lambda_1 \left(\nabla h \right)^2 - \lambda_2 \nabla^2 \left(\nabla h \right)^2 \tag{6}$$

The λ_1 term tends to disorder the pattern and λ_2 term induces the coarsening of

the structures§. The behaviour of Eq. (6) for different sputtering geometries has been theoretically studied in Refs. [33, 34]. It has been shown that Eq. (6), using approximate analytical predictions to estimate the parameters of the equation can quantitatively explain a set of experimental data [35].

Numerical analysis faces an obvious problem because the parameter space is extremely large. Up to now, these equations have been tested by comparison with ensemble averaged quantities like the pattern wavelength $\ell(t)$, the surface roughness $W(t)$ or the power spectrum density of the surface height. These quantities give information about statistical averages of the surface morphology at time t. But after the saturation regime has been reached, these averages do not change. Moreover, as we show below, depending on the set of parameters used, Eqs. (5) and (6) can yield similar qualitative behaviours of the wavelength and the roughness evolution (i.e. an exponential increase at early times followed by a saturation regime). Hence, it is arguable that the validity of the continuum models can be concluded from measurements of averaged quantities alone. However, as we illustrate in the following, the investigation of the system fluctuations during the saturation regime can help to discriminate between the two models because they predict different dynamical behaviours. Determining the models that govern the nanostructure growth will not only allow to understand better the fundamentals of the erosion induced pattern formation but may also help in the fabrication of well controlled nanostructure patterns.

We have simulated surface topographies at different sputtering times by numerical integration of Eqs. (5) and (6). We have used a forward-backward difference method in a 256×256 square lattice with periodic boundary conditions, combined with an Euler integration method for the time. Surfaces with uniformly distributed random heights have been used as initial conditions. The spatial and time steps were $\Delta x = 1$ and $\Delta t = 0.01$ respectively. The improved discretisation proposed by Lam & Shin [36] was used to calculate the non-linear terms of the equation. $W(t)$, the mean roughness of the surface at time t, is obtained by computing:

$$W(t) = \sqrt{\frac{1}{L_x L_y} \sum_{i,j=1}^{L_x, L_y} \left[h(i, j, t) - \bar{h}(t) \right]^2} \tag{7}$$

where $L_{x,y}$ denote the dimensions of the image (in pixels) and $\bar{h}$ is the mean height. The evolution of $W(t)$ for Eqs. (5) and (6) is shown in Figs. 1 (a) and (b), respectively. We note that in the present numerical example, although the evolution of the roughness is very different at the early times, in both cases a saturation regime is reached and in incoherent X-ray experiments the scattered signal would not evolve any further. Examples of the morphologies obtained at two different times after saturation of the roughness are shown in Fig. 2. The lateral and height scales are arbitrary.

To simulate the results of an XPCS experiment, each topography is Fourier transformed (FT) and multiplied by its conjugate to calculate the intensity in reciprocal

---

§ In formulas (5) and (6) we have used the same parameter symbols and signs as in Refs. [29] and [32]. Thus, $\mathcal{K}$ in Eq. (6) is equivalent to D_{eff} in Eq. (5). However, the signs of ν are inverted.

space. The normalised intensity fluctuations at a momentum transfer $\boldsymbol{q}$ are calculated in the following way:

$$D\left(\boldsymbol{q}, t\right) = \frac{I\left(\boldsymbol{q}, t\right) - \langle I\left(\boldsymbol{q}, t\right)\rangle}{\langle I\left(\boldsymbol{q}, t\right)\rangle} \tag{8}$$

$\langle I\left(\boldsymbol{q}, t\right)\rangle$ corresponds to the average intensity and is calculated by performing a radial average of all the speckle intensity values at equivalent $\boldsymbol{q}$ values. This procedure is valid only for isotropic systems. For non-isotropic systems the average intensity at a momentum transfer $\boldsymbol{q}$ can be obtained by a procedure described in Ref. [37]. For systems in equilibrium, the intensity fluctuations around the average value depend only on the time difference Δt between measurements but not on when the measurements have been made. One-time autocorrelation functions‖ are often used to analyse the fluctuations of equilibrium systems [38, 40]:

$$\zeta\left(\boldsymbol{q}, \Delta t\right) = \langle D\left(\boldsymbol{q}, t\right) D\left(\boldsymbol{q}, t + \Delta t\right)\rangle_{\boldsymbol{q},t} \tag{9}$$

and the average is done over pixels with equivalent momentum transfer and over time. The momentum transfer at which the measurements are done determines the length scales that are probed.

Sputtered surfaces are nonequilibrium systems whose dynamics can depend on the history or 'age' of the system under study. That is, the correlations that are measured at sputtering time t_a may be different from the correlations measured at a later time t_b. Therefore, the time average that is done when using one-time correlation functions cannot be performed. To study the fluctuations of non-equilibrium systems, two-time correlation functions (TTCF) should be used instead [40]:

$$\zeta\left(\boldsymbol{q}, t_1, t_2\right) = \langle D\left(\boldsymbol{q}, t_1\right) D\left(\boldsymbol{q}, t_2\right)\rangle \tag{10}$$

where the average is done over pixels with equivalent momentum transfer $\boldsymbol{q}$ but not over the time. The TTCFs evaluated from the models are shown in Fig. 3. Eqs. (5) and (6) predict that the roughness does not evolve anymore after $t \sim 100$ and has reached a saturation value in both cases (see Fig. 1). However, the predicted TTCFs are completely different after this time. The parameters we used to integrate Eq. (5) yield a chaotic spatiotemporal evolution of the surface morphology [29, 30], which is evidenced by the behaviour of the corresponding TTCF (Fig. 3 (a)): indeed, the TTCF decays very fast in the direction perpendicular to the $t_1 = t_2$ diagonal, which indicates that the amount of time in which successive patterns being formed at the surface are correlated is very short. Moreover, this correlation time does not evolve with sputtering time (i.e., distance along the $t_1 = t_2$ diagonal), showing that the dynamics are stationary. On the other hand, the behaviour of the TTCF of Eq. (6) is very different: the correlation of the patterns is maintained for some time (Fig. 3 (b)) and during IBS there is an aging effect, i.e., the correlation time increases with sputtering time, indicating that the system

‖ Time correlation functions are of common use to study time or frequency dependence phenomena. An introduction to time correlation functions applied to condensed matter can be found in [38] and diverse examples (diffusive systems, Brownian motion, spin systems, etc.) are described in Ref. [39].

displays nonequilibrium dynamics which become progressively slower. Ageing dynamics arise in many systems out-of-equilibrium such as glasses, granular media, colloidal gels, etc. [41]. We remark that the observation of the ageing behaviour is not accessible in any other way but through the use of time correlations. Two patterns can have the same ensemble averaged properties, and one pattern can be completely static, while the other one is dynamic. Measurements of the time correlations do distinguish between these two patterns, but measurements of ensemble averaged quantities do not.

The analysis of the intensity fluctuations serves to investigate the dynamics in the nonlinear saturation regime, once the pattern has been formed and far from the threshold and the linear regime of exponential amplification. The time correlation functions depend on the momentum transfer q (see Eqs. (9) and (10)) and give information about the temporal correlations occurring at the length scale $2\pi/|q|$ along the direction given by the vector q. For isotropic systems the vector character of q does not play a role and the time correlation functions depend on the modulus $|q|$ only. In the case of anisotropic systems, the time correlation functions obtained at a particular $|q|$ value also depend on the direction of q. XPCS is widely used to study diffusion constants and the hydrodynamic modes of flowing systems [27]. In that regard, information about ripple diffusion on surfaces sputtered at off-normal incidence could be accessed with XPCS from measurements of the intensity fluctuations performed at different q values. Moreover, XPCS may help to test the recently published generic hydrodynamic approach to describe the pattern formation on ion beam sputtered surfaces [17].

Some remarks concerning the experimental measurement of two-time correlation functions with XPCS are necessary. XPCS experiments are much more technically demanding than conventional GISAXS or GID measurements. First, using a coherent X-ray beam at a third generation synchrotron radiation source implies that only a small part of the full incoming beam can be used [22]. Consequently, the scattered signal is much weaker than in conventional GID or GISAXS experiments. Moreover, special care has to be taken with the different components along the beam path (optical elements, windows, slits etc.) because they can generate spurious speckles and degrade the beam [42]. In addition, as the experiment tries to obtain a dynamical information from the sample, any small movement or vibration from the system may affect the results and therefore an extremely stable setup is needed. A constraint of XPCS is that meaningful intensity fluctuation measurements can only be done at the saturation regime. In the regime of exponential amplification it is very difficult to correlate in time the intensities measured at the same momentum transfer at two different times because the correlation peak due to the lateral arrangement of the structures is shifting. XPCS gives access to the dynamics in the saturation regime but cannot disclose "how" and "when" this saturation occurs. That information is out of the reach of XPCS but can be obtained, for example, with GISAXS measurements [9]. Therefore, XPCS is complementary to other techniques. XPCS experiments have already been performed by the authors on the saturation regime of sputtered GaSb samples and will be reported elsewhere.

In summary, we have shown that the capability of the XPCS technique to investigate

the dynamics of a system in and out of equilibrium can be used to better understand the process of surface erosion. Especially, the determination of the TTCF can serve as a discriminator between models with comparable qualitative (asymptotic) predictions.

Acknowledgments

References

[1] Navez M, Sella C and Chaperot D 1962 *Comptes Rendus Acad. Sci.* **254** 240
[2] Facsko S, Dekorsy T, Koerdt C, Trappe C, Kurz H, Vogt A and Hartnagel H L 1999 *Science* **285** 1551
[3] Cuerno R, Vázquez L, Gago R and Castro M 2009 *J. Phys.: Cond. Matter* **21** 220301
[4] Carter G 2001 *J. Phys. D: Appl. Phys.* **34**, R1
[5] Valbusa U, Boragno C and Buatier de Mongeot F 2002 *J. Phys.: Cond. Matter* **14** 8153
[6] Chan W L and Chason E 2007 *J. Appl. Phys.* **101**, 121301
[7] Muñoz-García J, Vázquez L, Cuerno R, Sánchez-García J A, Castro M and Gago R. 2009 in: Toward Functional Nanomaterials, edited by Z. M. Wang, Lecture Notes in Nanoscale Science and Technology **5** (Springer, Heidelberg) chap. 10.
[8] Boragno C and Felici R 2009 *J. Phys.: Cond. Matter* **21** 224006
[9] Carbone D, Biermanns A, Ziberi B, Frost F, Plantevin O, Pietsch U and Metzger T H 2009 *J. Phys.: Cond. Matter* **21**, 224007
[10] Carter G and Vishnyakov V 1996 *Phys. Rev. B* **54** 17647
[11] Davidovitch B, Aziz M J and Brenner M P 2007 *Phys. Rev. B* **76** 205420
[12] Özaydin G, Ludwig K F Jr, Zhou H, Zhou L and Headrick R L 2008 *J. Appl. Phys.* **103** 033512
[13] Zhou H, Zhou L, Özaydin G, Ludwig K F Jr and Headrick R L 2008 *Phys. Rev. B* **78** 165404
[14] Madi C S, Anzenberg E, Ludwig K F Jr and Aziz M J 2011 *Phys. Rev. Lett.* **106** 066101
[15] Norris S A, Samela J, Bukonte L, Backman M, Djurabekova F, Nordlund K, Madi C S, Brenner M P and Aziz M J 2011 *Nature Comms.* **2:276**
[16] Cuerno R, Castro M, Muñoz-García J, Gago R and Vázquez 2011, *Nucl. Instrum. Meth. B* **269** 894
[17] Castro M and Cuerno R 2012, *Appl. Surf. Sci.* **258** 4171
[18] Shenoy V B, Chan W L and Chason E 2007 *Phys. Rev. Lett.* **98** 256101
[19] Shipman P D and Bradley R M 2011 *Phys. Rev. B* **84** 085420
[20] Bradley R M 2011 *Phys. Rev. B* **83** 195410
[21] Nugent K A (2010) *Adv. Phys.* **59** 1
[22] Lengeler B 2001 *Naturwissenschaften* **88** 249
[23] Sutton M, Nagler S E, Mochrie S G, Greytak T, Bermann L E, Held G, Stephenson G B 1991 *Nature* **352** 608
[24] Grübel G and Zontone F 2004 *J. Alloys Compd.* **362** 3
[25] Grübel G, Madsen A and Robert A 2008 in: Soft-Matter Characterization, edited by R. Borsali and R. Pecora (Springer, Berlin) chap. 18
[26] Sutton M 2008 *C. R. Physique* **9** 657
[27] Berne B J and Pecora R 2000 *Dynamic Light Scattering* Dover Publicaitons Inc. (New York)
[28] Schmidbauer M 2004 *X-ray Diffuse Scattering from Self-Organized Mesoscopic Semiconductor Structures* (Springer Tracts in Modern Physics vol. **199**). (Springer, Berlin)

[29] Facsko S, Bobek T, Stahl A, Kurz H and Dekorsy T 2004 *Phys. Rev. B* **64** 153412
[30] Paniconi M and Elder K R 1997 *Phys. Rev. E* **56** 2713
[31] Bradley R M 2011 *Phys. Rev. B* **83** 075404
[32] Castro M, Cuerno R, Vázquez L and Gago R 2005 *Phys. Rev. Lett.* **94** 016102
[33] Muñoz-García J, Castro M and Cuerno R 2008 *Phys. Rev. B* **78** 205408
[34] Muñoz-García J, Cuerno R and Castro M 2009 *J. Phys.: Cond. Matter* **21** 224020
[35] Muñoz-García J, Gago R, Vázquez L, Sánchez-García J A and Cuerno R 2010 *Phys. Rev. Lett.* **104** 026101
[36] Lam C H and Shin F G 1998 *Phys. Rev. E* **58** 5592
[37] Fluerasu A, Sutton M and Dufresne E 2005 *Phys. Rev. Lett.* **94** 055501
[38] Pecora R in 2008 in: Soft-Matter Characterization, edited by R. Borsali and R. Pecora (Springer, Berlin) chap. 1
[39] Chaikin P M and Lubensky T C (1995) *Principles of Condensed Matter Physics* Cambridge Univ. Press. (Cambridge)
[40] Sutton M, Laaziri K, Livet F and Bley F 2003 *Opt. Express* **11** 2268
[41] Barrat J-L, Feigelman M, Kurchan J and Dalibard J (2003) "Slow relaxations and nonequilibrium dynamics in condensed matter" EPD Sciences (Paris) and Springer (Berlin)
[42] Carbone D, Plantevin O, Gago R, Mocuta C, Bikondoa O, Alija A, Petit L, Djazuli H and Metzger T H 2008 *J. Synch Rad* **15** 414
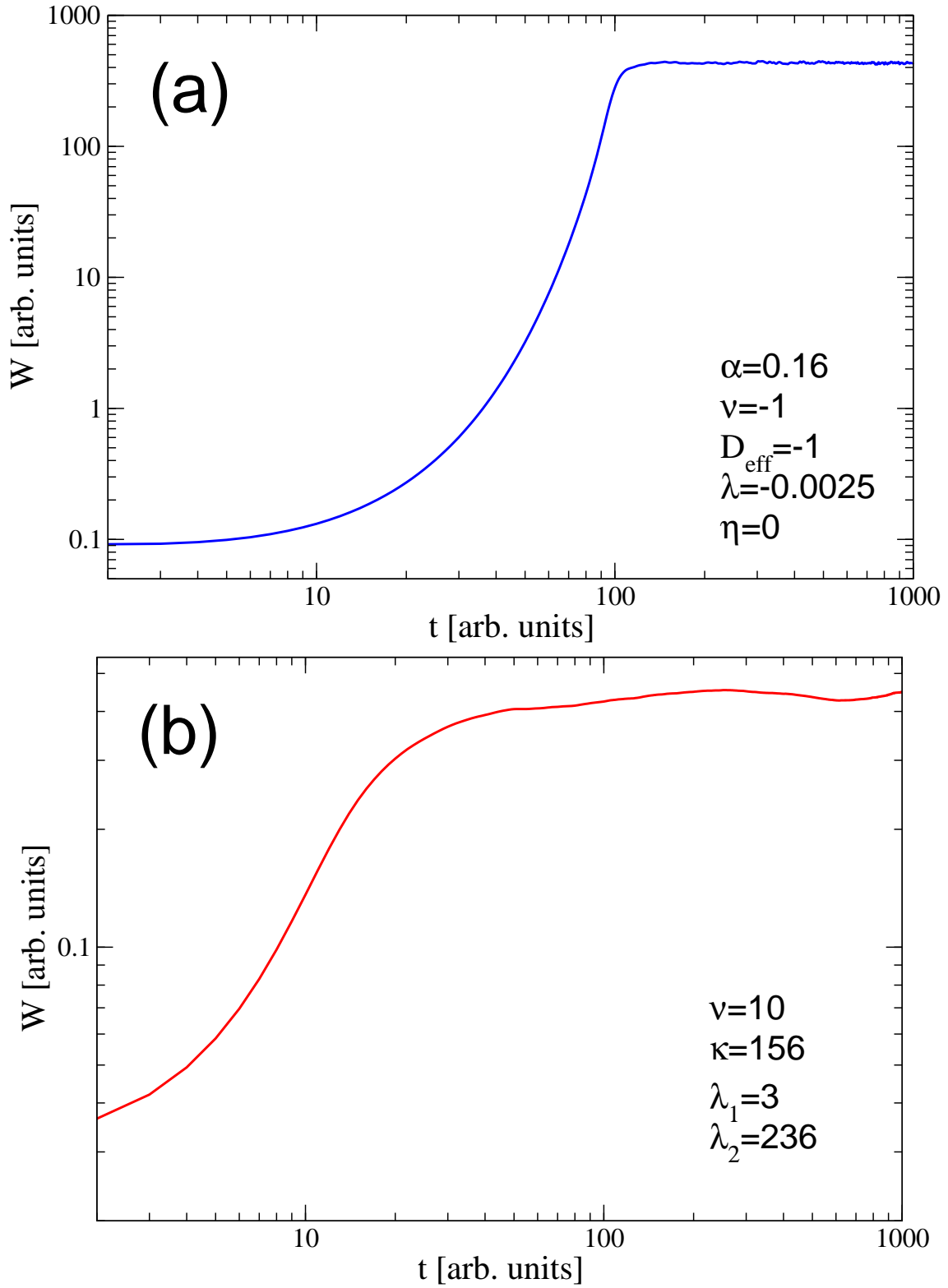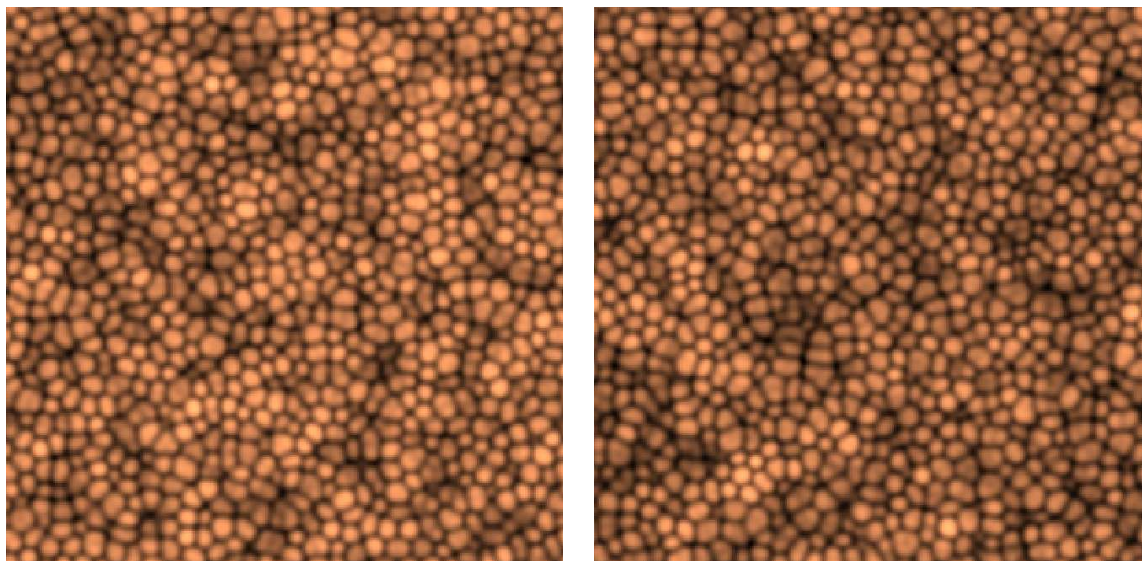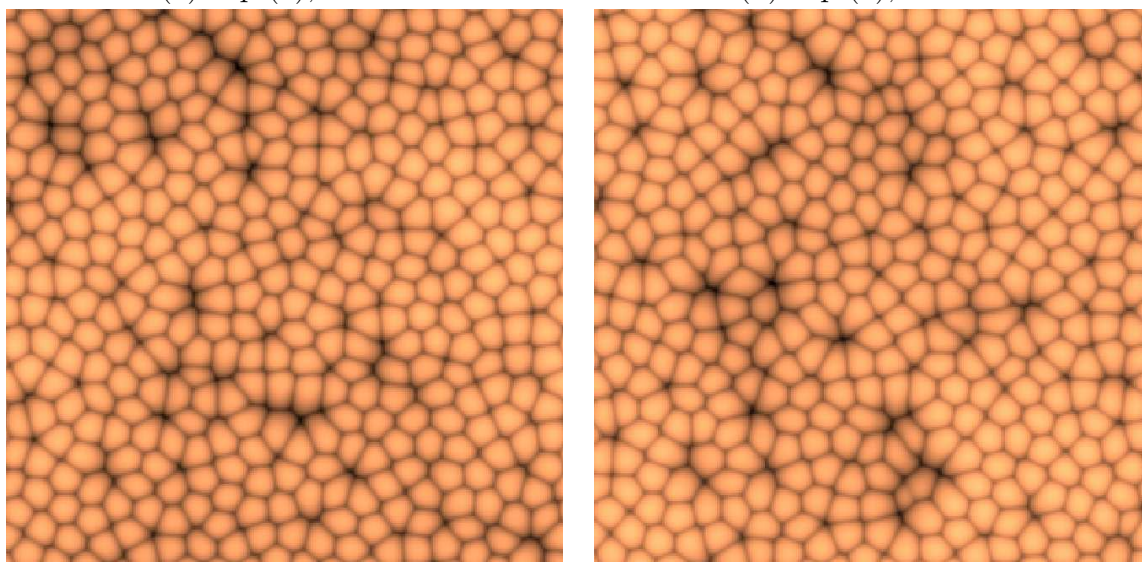
Figure 1. (Colour online) Evolution of the surface roughness W during IBS according to Eqs. (5) (panel (a)) and (6) (panel (b)). The parameters used to integrate the equations are displayed in the figures. Note that the scales are logarithmic to display better the early time evolution.

(a) Eq. (5), t=500

(b) Eq. (5), t=1000

(c) Eq. (6), t=500

(d) Eq. (6), t=1000

Figure 2. (Colour online) Examples of topographies at different times obtained by numerical integration of Eqs. (5) and (6), using the same parameters as for Figs. 1 (a) and (b). The lateral dimensions can be rescaled arbitrarily.
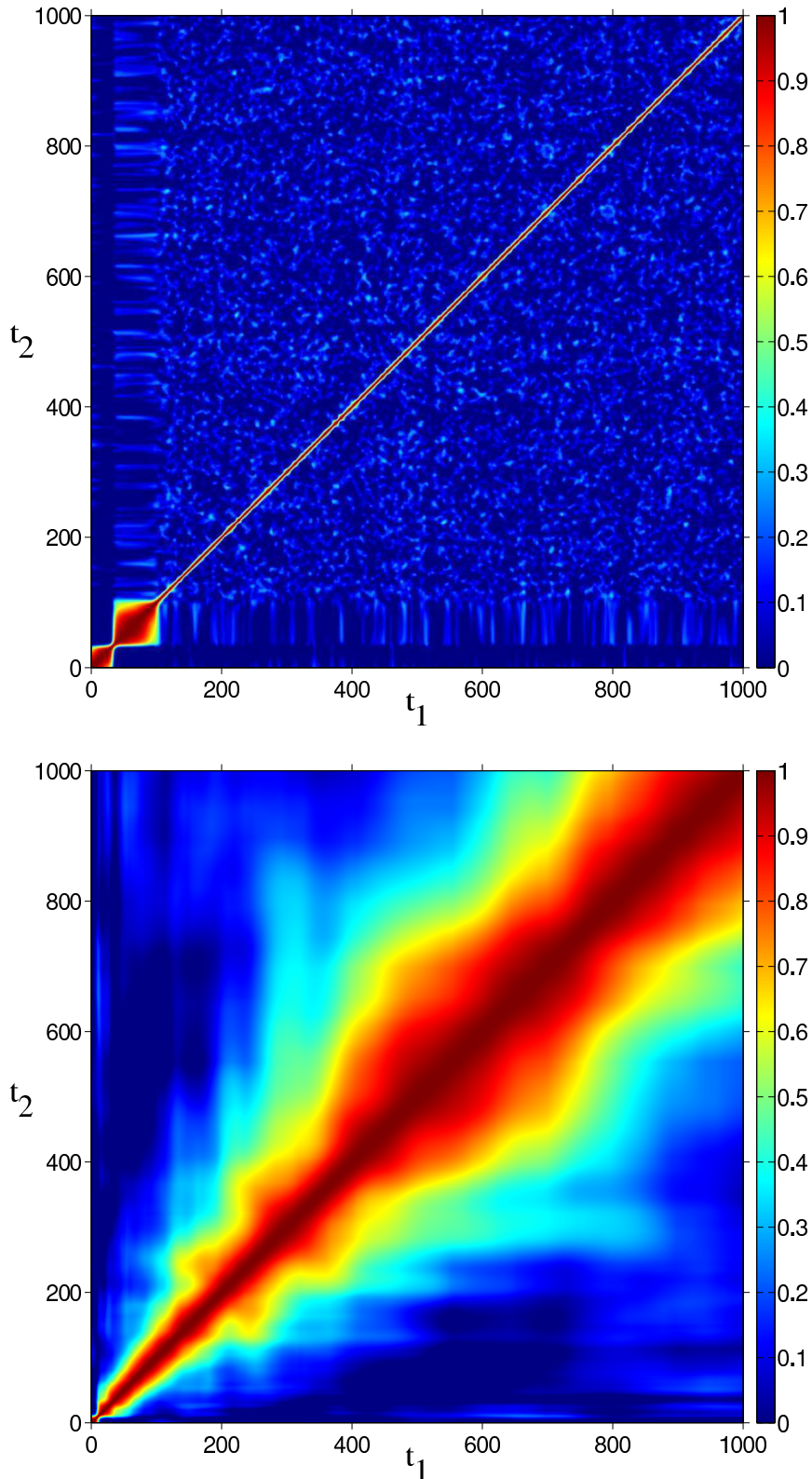
Figure 3. (Colour online) Contour plots of the scaled two-time correlation functions (TTCF) calculated using Eqs. (5) (top panel) and (6) (bottom panel), using the parameters indicated in Fig. 1, and calculated from the intensity fluctuations at the momentum transfer corresponding to the first spatial correlation peak. The TTCFs are usually described by two variables: the sputtering time or age $t_a = (t_1 + t_2)/2$, and the time difference $\Delta t = |t_1 - t_2|$, which is the distance from the $t_1 = t_2$ diagonal in the perpendicular direction. The correlation or decay time is defined as $\tau = \Delta t/2$ [25]. The time units are arbitrary. The colour scale corresponds to the contour levels.